


## RESEARCH ARTICLE

# Infrared Spectrum and UV-Triggered Transformations of Matrix-Isolated *Meta*-Fluorothiophenol Supported by Ground and Excited State Theoretical Calculations

A. J. Lopes Jesus<sup>1</sup> | J. R. Lucena Jr.<sup>2</sup> | G. P. Rodrigues<sup>3</sup> | G. Ogruc Ildiz<sup>4,5</sup> | S. A. do Monte<sup>3</sup>  | E. Ventura<sup>3</sup> | R. Fausto<sup>4,5</sup>

<sup>1</sup>CQC-IMS, Faculty of Pharmacy, University of Coimbra, Coimbra, Portugal | <sup>2</sup>Departamento de Química, CCT, Universidade Estadual da Paraíba, Campina Grande, Brazil | <sup>3</sup>Departamento de Química, CCEN, Universidade Federal da Paraíba, João Pessoa, Brazil | <sup>4</sup>CQC-IMS, Department of Chemistry, University of Coimbra, Coimbra, Portugal | <sup>5</sup>Department of Physics, Faculty Sciences and Letters, Istanbul Kultur University, Istanbul, Turkey

**Correspondence:** A. J. Lopes Jesus ([ajorge@ff.uc.pt](mailto:ajorge@ff.uc.pt)) | E. Ventura ([elizete@quimica.ufpb.br](mailto:elizete@quimica.ufpb.br))

**Received:** 31 October 2024 | **Revised:** 23 December 2024 | **Accepted:** 27 December 2024

**Funding:** This work was supported by Project PTDC/QUI-QFI/1880/2020, funded by National Funds via the Portuguese Foundation for Science and Technology (FCT), and by the European research Agency via the European Research Agency ERA-Chair 1011848998 Spectroscopy@IKU “Manipulating and Characterizing Molecular Architectures: From Isolated Molecules to Molecular Crystals”. The Coimbra Chemistry Centre—Institute of Molecular Sciences (CQC-IMS) is supported by FCT through projects UIDB/00313/2020 and UIDP/00313/2020, co-funded by COMPETE and the IMS special complementary funds provided by FCT. The authors also acknowledge the Laboratory for Advanced Computing at University of Coimbra (<https://www.uc.pt/lca>) for providing computing resources and LaserLab Coimbra for experimental facilities. A. J. Lopes Jesus and J. R. Lucena Jr. would like to thank Igor Reva for his invaluable help with the matrix-isolation experiments and for insightful discussions in the early stages of this work. E. Ventura and S. A. do Monte. thank the Brazilian agency CNPq (Grant Numbers 308371/2021-6, and 313398/2023-2) for support. E. Ventura, S. A. do Monte, J. R. Lucena Jr. and G. P. Rodrigues thank funding from the National Institute of Science and Technology on Molecular Sciences (INCT-CiMol) (Grant CNPq 406804/2022-2 and fellowships 153685/2024-7), CAPES, the Laboratório Nacional de Computação Científica—LNCC for the computational facilities of the Santos Dumont (SDumont) supercomputer cluster and the Brazilian agency FINEP for financial support.

**Keywords:** matrix isolation | *meta*-fluorothiophenol | multireference/multiconfigurational methods | photochemistry | phototautomerization | reversibility | thiones

## ABSTRACT

The infrared (IR) spectrum of *meta*-fluorothiophenol (mFTP) isolated in a low-temperature N<sub>2</sub> matrix was recorded and interpreted with the aid of B3LYP vibrational frequency calculations for both *cis* and *trans* conformers. Then, photochemical transformations in the matrix-isolated compound were triggered through UV–Vis laser irradiations and their outcomes were monitored by IR spectroscopy. Upon excitation at  $\lambda = 285$  nm, thiol-to-thione phototautomerization was identified as the sole reaction pathway, leading to the formation of three thione isomers. Among them, the *ortho*-isomer where the hydrogen atom reattaches to the fluorine-substituted side of the aromatic ring was identified as the predominant photoproduct. Identification of the photoproducts was confirmed by comparing the emerging experimental spectra with the IR absorptions predicted for the candidate structures. The photoreaction was found to be reversible, as irradiation at  $\lambda = 405$  nm partially restored the reactant. The experimental results were complemented with the application of multireference/multiconfigurational (CASSCF, CASPT2, MR-CIS) and TD-DFT (TD-M062X,  $\omega$ B97XD, and  $\tau$ -HCTHhyb) methods to investigate the excited state properties of mFTP, including the simulation of its UV photoabsorption spectra. A comparative analysis of the results obtained by the different methods was performed. This combined experimental and theoretical approach provided valuable insights into the photochemical behavior and electronic structure of fluorinated thiophenols.

## 1 | Introduction

The intriguing excited state properties of thiophenol and its derivatives have stimulated extensive research to elucidate the photochemical behavior of this class of molecules [1–11]. This interest is mainly driven by their role in elucidating non-adiabatic coupling phenomena and hydrogen transfer reactions, which are key processes in biological, atmospheric and material sciences [12–14]. Upon UV excitation, these molecules typically undergo homolytic cleavage of the S–H bond, leading to the formation of phenylthiyl radicals [2, 15], which play a central role in subsequent photochemical reactions. This photoprocess has been shown to proceed through a  $\pi\sigma^*$  mediated mechanism, similar to that reported for phenols and other aromatic compounds [13]. A combination of theoretical approaches [4–7, 15, 16] and experimental techniques, such as time-resolved spectroscopy [17] and photofragment translational spectroscopy [2, 7, 8], has been employed to uncover the dynamics driving the photodissociation of thiophenols.

Matrix-isolation IR spectroscopy coupled with UV-excitation sources has also proven to be a powerful method for investigating the photochemical behavior of thiophenols [11, 18] and related compounds [19–24]. By trapping molecules in a cryogenic matrix, this technique stabilizes and enables the detailed spectroscopic characterization of the photogenerated species, including short-lived intermediates that are challenging to detect under other experimental conditions, thereby offering valuable insights into reaction mechanisms [21, 25, 26]. The phototransformations of parent thiophenol isolated in a low-temperature Ar matrix has been investigated in our laboratory [11]. The main observed transformation was the thiol-to-thione phototautomerization, involving migration of the H-atom from the S–H bond to the *ortho* and *para* carbon atoms of the aromatic ring. The generated thione isomers, alongside the intermediate phenylthiyl radical, were identified spectroscopically.

The findings on the parent thiophenol molecule led us to extend our research to thiophenol derivatives to investigate how the phenyl ring substitution influences their photochemical behavior. While a reasonable number of studies utilizing theoretical calculations [27–30], gas-phase photochemistry [8, 10, 29], and solution-phase photolysis [31] have been conducted on different substituted thiophenols, matrix isolation studies on these compounds are comparatively scarce. To date, only the photochemistry of 2-chloro-substituted thiophenol isolated in Ne and Ar matrices has been investigated [18]. For this molecule, two reaction pathways have been identified. In a Ne matrix, a five-membered-ring thioketone compound was identified as the major photoproduct, resulting from a reaction analogous to the Wolff rearrangement [21]. In contrast, in an Ar matrix, *ortho*- and *para*-thione isomers were found to be the predominant photoproducts, consistent with findings for the parent thiophenol [11].

In the present study, we investigated the UV–Vis-induced photochemistry of *meta*-fluorothiophenol (mFTP) isolated in a low-temperature  $N_2$  matrix. To support the experimental findings, full geometry optimizations and vibrational calculations were performed on the ground state of the reactant and candidate photoproducts. Furthermore, TD-DFT and higher-level theoretical methods were employed to analyze the excited-state

properties of mFTP and its thione isomer photoproducts, including vertical excitation energies, oscillator strengths, and relevant electronic configurations. This analysis was extensively applied to mFTP, where a comparison was conducted among various multireference/multiconfigurational (CASSCF, CASPT2, MR-CIS) and TD-DFT (TD-M062X,  $\omega$ B97XD, and  $\tau$ -HCTHhyb) methods. Additionally, simulations of the photoabsorption spectra were performed for this molecule in both the gas phase and in solution.

## 2 | Methods

### 2.1 | Experimental Methods

Commercial mFTP **1**, purchased from Sigma-Aldrich (98%), was used in the matrix-isolation experiments. Before usage, the liquid compound underwent several freeze-pump-thaw cycles to remove volatile impurities. The methodology for preparing the low-temperature matrices followed the approach previously employed in experiments with *meta*-fluorophenol [23]. The compound and the  $N_2$  matrix host gas (N60, Air Liquide) were premixed monometrically in a 2 L Pyrex reservoir, maintaining a guest-to-host molar ratio of approximately 1:600. Then, the room temperature gaseous mixture was deposited onto an optical CsI substrate, cooled to 16 K by an APD Cryogenics DE-202A closed-cycle refrigerator. The temperature of the cold window was measured directly at the sample holder with an accuracy of 0.1 K by using a silicon diode sensor connected to a digital controller (Scientific Instruments, Model 9650-1). Mid-infrared spectra (4000–400  $cm^{-1}$ ) of matrix-isolated **1** were recorded with a resolution of 0.5  $cm^{-1}$  using a Thermo Nicolet 6700 Fourier-transform infrared (FTIR) spectrometer equipped with a Ge/KBr beam splitter and a deuterated triglycine sulphate (DTGS) detector. UV–Vis-induced processes in matrix-isolated **1** were investigated by irradiating the frozen sample through the outer quartz window of the cryostat with monochromatic (spectral width = 0.2  $cm^{-1}$ ) radiation at different wavelengths in the 425–285 nm range. The radiation was generated by the frequency-doubled signal beam of a Quanta-Ray MOPO-SL optical parametric oscillator (OPO), which was pumped by a pulsed Nd:YAG laser pro 230 from Spectra-Physics (repetition rate = 10 Hz, pulse energy ~1–3 mJ, duration = 10 ns).

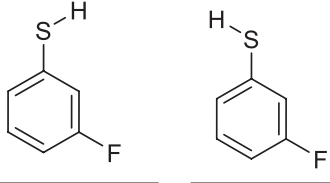
### 2.2 | Computational Methods

The ground state geometries of mFTP **1** and of the species resulting from its UV-induced photochemistry were fully optimized using the Density Functional Theory (DFT), specifically employing the B3LYP [32–34] functional with the 6-311++G(2d,2p) basis set [35]. At the optimized geometries, harmonic, and in some specific cases, anharmonic vibrational calculations were performed at the same level of theory. For a clearer graphical comparison with the experimental spectra, the calculated harmonic wavenumbers, scaled by 0.98 or 0.96 for the regions below or above 3000  $cm^{-1}$ , respectively, and IR intensities (in  $km\ mol^{-1}$ ), were convoluted using Lorentzian functions. A full width at half-maximum (FWHM) of 2  $cm^{-1}$  was applied, and the peak heights were adjusted to match the calculated IR intensities. This convolution process was performed using the

Chemcraft software [36]. For **1**, additional full geometry optimizations calculations were carried out using both the B3LYP (including vibrational frequency calculations) and MP2 [37] methods in conjunction with the aug-cc-pVTZ basis set [38]. The Cartesian coordinates of the fully optimized geometries of the species relevant to this study (all exhibiting  $C_s$  symmetry) are provided in Tables S1 and S2, while the respective computed vibrational data are given in Tables S3–S5. All the above calculations were carried out using the Gaussian 16 program package (version B.01) [39].

Excited-state calculations were performed in mFTP **1c** (see top of Table 1) using multiconfigurational methods Complete

**TABLE 1** | Relative energies ( $\Delta E_{el}$ ,  $\Delta E_0$ , and  $\Delta G$ ), equilibrium populations (Pop.) at 298.15 K and dipole moments ( $\mu/D$ ) calculated for the *cis* and *trans* conformers of mFTP **1** (**1c** and **1t**), along with the energy barriers for their interconversion ( $\Delta E_{el}^\ddagger$ ), calculated at different levels of theory.<sup>a</sup>

Level of theory		
	<b>1c</b>	<b>1t</b>
B3LYP/6-311++G(2d,2p)		
$\Delta E_{el}$	0.00	-0.01
$\Delta E_0$	0.00	0.01
$\Delta G$	0.00	0.17
Pop.	51.7	48.3
$\mu$	0.67	2.18
$\Delta E_{el}^\ddagger$	4.49	4.50
B3LYP/aug-cc-pVTZ		
$\Delta E_{el}$	0.00	-0.04
$\Delta E_0$	0.00	-0.02
$\Delta G$	0.00	0.08
Pop.	50.8	49.2
$\mu$	0.64	2.09
$\Delta E_{el}^\ddagger$	5.64	5.67
MP2/aug-cc-pVTZ		
$\Delta E_{el}$	0.00	-0.08
$\mu$	0.75	2.35
$\Delta E_{el}^\ddagger$ <sup>b</sup>	3.35	3.35

<sup>a</sup>All energies are given relative to **1c** and are reported in  $\text{kJ mol}^{-1}$ .  $\Delta E_{el}$  represents the relative electronic energy,  $\Delta E_0$  includes correction for the zero-point vibrational energy and  $\Delta G$  denotes the relative Gibbs energy at 298 K. Equilibrium populations (Pop.) were estimated at 298.15 K by means of the Boltzmann distribution based on the  $\Delta G$  values. The energy barriers ( $\Delta E_{el}^\ddagger$ , in  $\text{kJ mol}^{-1}$ ) exclude the contribution of the zero-point vibrational energy and represent the energy difference between the first-order transition state and the respective local minimum.

<sup>b</sup>Taken from Reference [8].

Active Space Self-Consistent Field Method (CASSCF) and Multireference Configuration Interaction with single excitation (MR-CIS) using COLUMBUS program [40–42], the Complete Active Space with Second-Order Perturbation Theory (CASPT2) using the Turbomole program [43], as well as the time-dependent density functional theory (TD-DFT) using Gaussian 16 (version C.01) [44]. The  $\omega$ B97XD [45], M06-2X [46], and  $\tau$ -HCTHhyb [47] functionals were selected based on previous results obtained for similar systems such as thiophenol [28]. The aug-cc-pVDZ basis set [48, 49] was used for all excited state calculations. Three singlet excited states were computed at  $C_s$  symmetry for mFTP **1**, where an active space consisting of 12 electrons and 11 orbitals [CAS(12,11)] was considered. The plots of the molecular orbitals contained in the active space are given in Table S7. UV photoabsorption spectrum simulations of mFTP **1** in the region up to 5.5 eV were carried out in the gas phase, and solvent (*n*-hexane) using the CPCM model [50], characterizing the spectral band composed by the states of interest in this study. A comparison with experimental results from the literature was also carried out. These calculations have been performed at the TD-DFT level (with the  $\tau$ -HCTHhyb functional) using Newton-X [51] interfaced with Gaussian 16. The initial conditions to generate the absorption spectrum were computed with the nuclear ensemble approach [52], sampling a quantum harmonic oscillator Wigner distribution with 500 points, which provides absolute intensities and bandwidths but does not include vibrational resolution.

### 3 | Results and Discussion

#### 3.1 | Structure and IR Spectrum of Matrix-Isolated mFTP

mFTP **1** exists in two conformers, *cis* (**1c**) and *trans* (**1t**), which differ on the orientation of the S–H bond, as illustrated in the top of Table 1. This table summarizes the results of theoretical calculations carried out for the two conformers at different levels of theory. The Cartesian coordinates of the geometries fully optimized at several levels are given in Table S1. To maximize the conjugation between the sulfur atom's lone pair (with *p*-character) and the  $\pi$ -system of the aromatic ring, for both optimized geometries the S–H bond and the phenyl ring are in the same plane leading to a  $C_s$  symmetry. As expected, conformer **1t**, with aligned S–H and C–F bond dipoles, has a larger electric dipole moment ( $\mu = 2.1$ – $2.4$  D) compared to **1c** ( $\mu = 0.6$ – $0.7$  D). In contrast to the *ortho*-substituted fluorothiophenol, where an intramolecular S–H...F hydrogen bond stabilizes the *cis* relative to the *trans* conformer [8, 53], no such bond is present in **1**. Therefore, the energy difference between the two rotamers is predicted to be extremely small at all levels of theory, typically less than  $0.1 \text{ kJ mol}^{-1}$ , regardless of whether electronic energy, zero-point corrected energy, or Gibbs free energy at 298 K is considered (see Table 1). These minor energy differences indicate that the two conformers are energetically degenerate, in line with the results of previous calculations performed for this molecule [8]. From an experimental point of view, this suggests that, prior to the  $N_2$  matrix deposition, the gaseous mixture should contain nearly equal proportions of both conformers.

In addition to the energy differences, the rotamerization barriers connecting the two conformers ( $\Delta E_{el}^\ddagger$ ) have been also computed

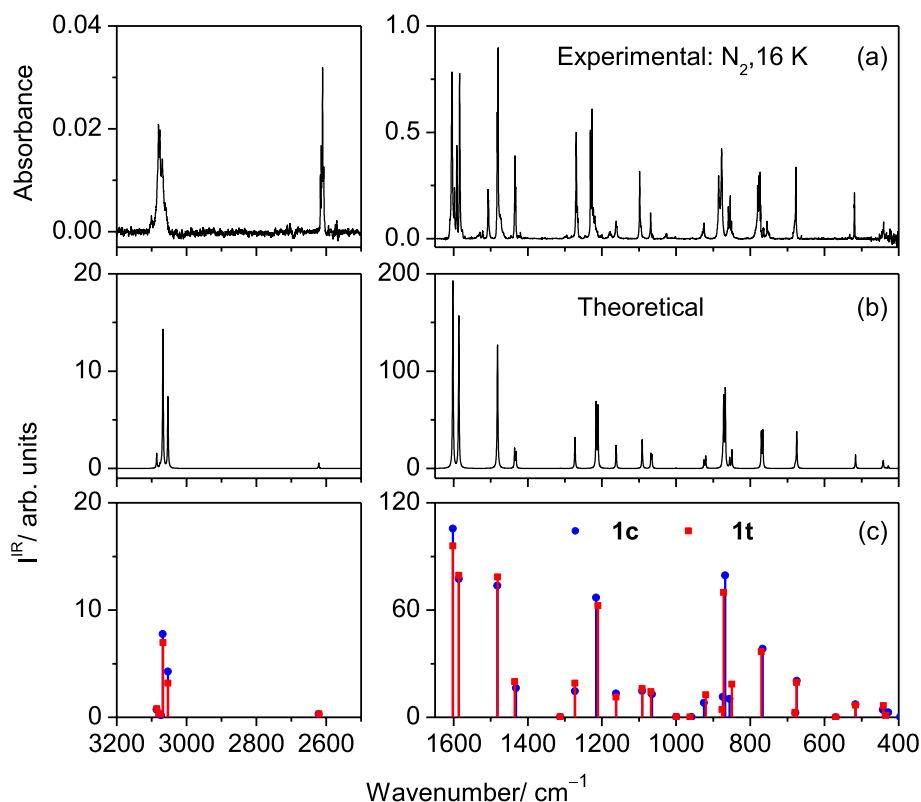
at the B3LYP level and are included in Table 1. The obtained values range from 4.5–5.7 kJ mol<sup>-1</sup>. A slightly lower rotamerization barrier was computed for this molecule at the MP2/aug-cc-pVTZ level (3.4 kJ mol<sup>-1</sup>) [8], which is comparable to the value reported for the unsubstituted thiophenol molecule (3.2 kJ mol<sup>-1</sup>) [2]. This is in agreement with previous theoretical studies carried by some of the authors of this work, which showed that the *meta*-substitution has no significant effect on the electron density distribution in the thiophenol core [54]. Despite the fact that the computed rotamerization barriers are sufficiently low to be crossed in a low-temperature matrix [55–57], the degeneracy between **1c** and **1t** suggests that both rotamers should exist in equilibrium in the deposited N<sub>2</sub> matrix [56].

Figure 1a presents the experimental IR spectrum of monomers of **1** isolated in solid N<sub>2</sub> at 16 K in the 3200–2500 and 1650–400 cm<sup>-1</sup> regions. This experimental spectrum is closely reproduced by the theoretical IR spectrum of the molecule (Figure 1b), which was generated using the vibrational data computed for the two conformers (represented in Figure 1c).

Based on the comparison between the experimental and theoretical spectra, an assignment of the observed IR bands to the corresponding computed vibrations was made, as detailed in Table 2. The structural and energetic similarity between **1c** and **1t** is also reflected in their calculated IR spectra. As depicted in Figure 1c and Table 2, the IR peaks of the two conformers either overlap or appear at very close wavenumbers, making it

difficult to definitively assign specific bands to each conformer. Nonetheless, the doublet pattern observed in certain experimental bands, which is also accurately reproduced in the theoretical spectra (see Figure S1 for additional details), suggests that both conformers co-exist in the frozen N<sub>2</sub> matrix, in line with the theoretical predictions.

Out of the 33 normal modes predicted for **1**, 23 have A' symmetry, while 10 have A'' symmetry. The fingerprint region of the experimental IR spectrum is dominated by the features at 1604, 1591/1584, 1482/1480, 1231/1227, and 886/877 cm<sup>-1</sup>. The corresponding theoretical peaks are predicted respectively at 1602.2, 1586.0, 1481.2, 1211.0, and 871.8 cm<sup>-1</sup> for **1c**, and at 1601.8, 1586.0, 1482.1, 1215.8, and 867.5 cm<sup>-1</sup> for **1t**. The first two bands are assigned to aromatic C–C ring stretching modes ( $\nu$ CC), while the third one is assigned to a mixture of in-plane CH bending ( $\delta$ CH) and  $\nu$ CC vibrations. The fourth band is mostly assigned to the C–F stretching vibration ( $\nu$ CF), with minor contributions of  $\nu$ CC and  $\delta$ CH, while the fifth is associated with ring deformation ( $\delta$ R) with a minor contribution of  $\nu$ CF. The higher frequency region of the IR spectrum is dominated by a set of weak bands: those in the 3110–3050 cm<sup>-1</sup> are assigned to the CH stretching vibrations ( $\nu$ CH), while that at 2611 cm<sup>-1</sup> corresponds to the SH stretching vibration ( $\nu$ SH), closely matching the  $\nu$ SH band observed at 2610 cm<sup>-1</sup> in the IR spectrum of unsubstituted thiophenol isolated in an Ar matrix [11]. The intensification of this band relative to the theoretical predictions can likely be attributed to the formation of S–H...N<sub>2</sub>



**FIGURE 1** | (a) Experimental IR spectrum recorded shortly after isolating monomers of mFTP **1** in an N<sub>2</sub> matrix at 16 K (3200–2500 and 1650–400 cm<sup>-1</sup> regions); (b) simulated 1:1 sum spectrum based on the B3LYP/6-311++G(2d,2p) vibrational data calculated for the *cis* (**1c**) and *trans* (**1t**) conformers (wavenumbers above and below 3000 cm<sup>-1</sup> were scaled by 0.960 and 0.980, respectively [the spectrum simulation was performed as described in Section 2.2]); (c) Wavenumbers (scaled) and IR intensities (unscaled) calculated for the two conformers. The experimental band at 1507 cm<sup>-1</sup> has no correspondence in the theoretical spectra. Its tentative assignment is provided in the caption of Table 2.

**TABLE 2** | Bands observed in the IR spectrum of mFTP **1** isolated in N<sub>2</sub> at 16 K, compared with the harmonic wavenumbers ( $\tilde{\nu}/\text{cm}^{-1}$ ) and absolute intensities ( $A^{\text{th}}/\text{km mol}^{-1}$ ) calculated for the *cis* (**1c**) and *trans* (**1t**) conformers at the B3LYP/6-311++G(2d,2p) level of theory, along with an approximate description of the vibration modes.

Experimental (N <sub>2</sub> , 16 K) <sup>a</sup>		Calc. 1c		Calc. 1t		Approximate description <sup>c</sup>
$\tilde{\nu}$	Int.	$\tilde{\nu}^{\text{b}}$	$A^{\text{th}}$	$\tilde{\nu}^{\text{b}}$	$A^{\text{th}}$	
A' modes						
3101	vw	3085.5	0.8	3085.6	0.7	$\nu\text{C4H} + \nu\text{C5H}$
3084 (sh)	vw	3076.1	0.3	3073.2	0.2	$\nu\text{C2H}$
3080/3076	w	3067.2	7.0	3067.9	7.8	$\nu\text{C5H} + \nu\text{C6H}$
3069	w	3053.3	3.2	3053.3	4.3	$\nu\text{C5H} - \nu\text{C6H}$
2611 (multiplet)	vw	2621.0	0.3	2621.6	0.3	$\nu\text{SH}$
1604 (s)	vs	1602.2	95.8	1601.8	105.6	$\nu\text{CC}$
1591/ <b>1584</b>	vs	1586.0	79.3	1586.0	77.3	$\nu\text{CC}$
1507	w	—	—	—	—	—
1482/ <b>1480</b>	vs	1481.2	78.5	1482.1	73.5	$\delta\text{CH}; \nu\text{CC}$
<b>1435</b> /1433	m	1435.6	19.9	1431.9	16.3	$\nu\text{CC}; \delta\text{CH}$
n.o.	—	1312.4	0.3	1312.5	<0.1	$\nu\text{CC}; \delta\text{CH}$
1269	m	1273.0	19.1	1272.5	14.6	$\nu\text{CC}; \delta\text{CH}$
1231/ <b>1227</b>	s	1211.0	62.4	1215.8	67.0	$\nu\text{CF}; \nu\text{CC}; \delta\text{CH}$
1162	w	1162.0	11.2	1161.6	13.3	$\delta\text{CH}$
1098	m	1091.7	16.1	1091.4	14.7	$\nu\text{CC}; \delta\text{CH}; \delta\text{CS}$
1069	w	1068.0	14.4	1065.4	12.8	$\nu\text{CC}; \delta\text{CH}$
1002	vw	1000.0	0.3	999.4	0.2	$\delta\text{R}$
925 (multiplet)	w	920.2	12.6	924.9	8.1	$\delta\text{SH}$
886/ <b>877</b>	s	871.8	69.8	867.5	79.3	$\delta\text{R}; \nu\text{CF}$
680 (sh)	vw	679.5	2.7	678.2	2.5	$\delta\text{R}; \nu\text{CC}; \nu\text{CF}$
519	w	516.2	6.8	516.4	7.2	$\delta\text{R}$
n.i.	—	434.7	0.9	428.0	2.7	$\delta\text{CF} - \delta\text{CS}$
n.i.	—	386.6	0.6	396.1	0.2	$\nu\text{CS}$
n.i.	—	227.9	2.4	226.6	0.1	$\delta\text{CF} + \delta\text{CS}$
A'' modes						
n.o.	—	962.6	0.2	958.5	<0.1	$\tau\text{R}; \gamma\text{CH}$
886/ <b>877</b>	s	876.2	4.3	874.3	11.4	$\gamma\text{CH}$
859/ <b>854</b>	w	849.6	18.5	855.7	10.3	$\tau\text{R}; \gamma\text{CH}$
774 (multiplet)	m	770.3	36.7	766.4	38.3	$\tau\text{R}; \gamma\text{CH}$
677	m	675.2	19.5	674.7	20.4	$\tau\text{R}$
n.o.	—	569.1	<0.1	569.6	<0.1	$\tau\text{R}$
441	w	441.4	6.6	442.7	4.2	$\tau\text{R}$
n.i.	—	231.0	0.6	231.4	<0.1	$\gamma\text{CF}; \tau\text{R}$
n.i.	—	176.1	1.4	175.7	1.7	$\gamma\text{CS}$
n.i.	—	92.4	13.3	100.4	12.5	$\gamma\text{SH}$

Note: A band observed at 1597 cm<sup>-1</sup> (not perceptible in Figure 1), is due to traces of monomeric water present in the matrix, while a band at 1507 cm<sup>-1</sup>, without no correspondence in the theoretical spectra, can be tentatively assigned to a Fermi Resonance between the fundamental at 1480 cm<sup>-1</sup> and a combination band predicted at 1485 cm<sup>-1</sup> by the anharmonic calculations (391.9 + 1092.9 cm<sup>-1</sup>,  $A^{\text{th}} = 19 \text{ km mol}^{-1}$ ).

Abbreviations: n.i. = not investigated; n.o. = not observed. Experimental intensities (Int.) are expressed qualitatively: m = medium; s = strong; vs = very strong; vw = very weak; w = weak.

<sup>a</sup>Experimental wavenumbers are given in cm<sup>-1</sup>. For the doublet bands, the most intense component is highlighted in bold.

<sup>b</sup>Calculated harmonic wavenumbers were multiplied by 0.960 (above 3000 cm<sup>-1</sup>) or 0.980 (below 3000 cm<sup>-1</sup>).

<sup>c</sup> $\nu$ , stretching;  $\delta$ , in-plane bending;  $\gamma$ , out-of-plane bending;  $\tau$  = torsion. Signs “+” and “-” designate combination of vibrations occurring in the same phase and in the opposite phase, respectively.

interactions that polarize the S–H bond. This is consistent with previously reported effects of this type of interactions on the vibrational intensities of hydrogen-bond donors (e.g., OH or SH groups) [58, 59].

### 3.2 | UV-Induced Transformations

To investigate the photochemical behavior of matrix-isolated **1**, the freshly deposited N<sub>2</sub> matrix was irradiated with narrow-band UV light from the OPO/laser system, and the potential phototransformations were monitored after each irradiation by recording an IR spectrum. These irradiations were conducted at a wavelength of 285 nm as it closely matches the experimentally determined long-wavelength absorption limit of this compound in hexane solution ( $\lambda = 290$  nm) [8] and its theoretically predicted long-wavelength absorption limit in both gas phase and solution (see Section 3.4 for details). In addition, it aligns with the wavelength range (290–287 nm) previously used in our laboratory to induce unimolecular photoreactions in thiophenol isolated in a low-temperature Ar matrix [11].

Exposure of matrix-isolated **1** to UV radiation at  $\lambda = 285$  nm for approximately 2 min resulted in a significant decrease in the intensity of its IR bands, with ~60% of the reactant being consumed (see Figure S2). This decrease was accompanied by the appearance of new bands, indicating the formation of photoproducts. The spectral changes are depicted in the difference spectrum shown in Figure 2a where the positive bands correspond to the photogenerated species and the negative ones to the reactant **1**. Based on the established photochemical behavior of thiophenol [11] and related compounds, such as phenol [19] and substituted phenols [21, 23, 60, 61] under matrix-isolated conditions, the most likely process induced by the UV excitation is the thiol  $\rightarrow$  thione tautomerization, involving a hydrogen-atom transfer from the SH group to a carbon atom on the aromatic ring. Notably, the energy introduced into mFTP **1** by these irradiations is  $\sim 420$  kJ mol<sup>-1</sup>, which exceeds the experimentally determined and calculated values for the S–H bond dissociation enthalpy in this compound (335–338 kJ mol<sup>-1</sup>) [8, 62, 63]. This reaction can produce three isomeric forms of thione, depending on the specific carbon atom to which the hydrogen reattaches after detaching from the SH group (Scheme 1). Two of these isomers, 5-fluorocyclohexa-2,4-diene-1-thione (**3a**) and 3-fluorocyclohexa-2,4-diene-1-thione (**3b**), arise from hydrogen reattachment at the two *ortho*-positions, either on the fluorine-substituted side of the ring or the opposite side, respectively. The third isomer, 3-fluorocyclohexa-2,5-diene-1-thione (**3c**), is formed when the hydrogen reattaches at the *para*-position.

To spectroscopically confirm the occurrence of thiol  $\rightarrow$  thione tautomerization, the structures of the three possible thione isomers were fully optimized at the B3LYP/6–311++G(2d,2p) level of theory (their relative and total energies are provided in Table S6). Vibrational data for the fully optimized structures were computed and compared with the experimental difference spectrum, as illustrated in Figure 2 (see also Tables S4 and S5 for details).

In order to obtain a better fit to the experimental data, the intensities of the photoproducts **3a**, **3b**, **3c**, and **2** (the *meta*-fluorophenylthiyl radical, discussed below) in both the simulated

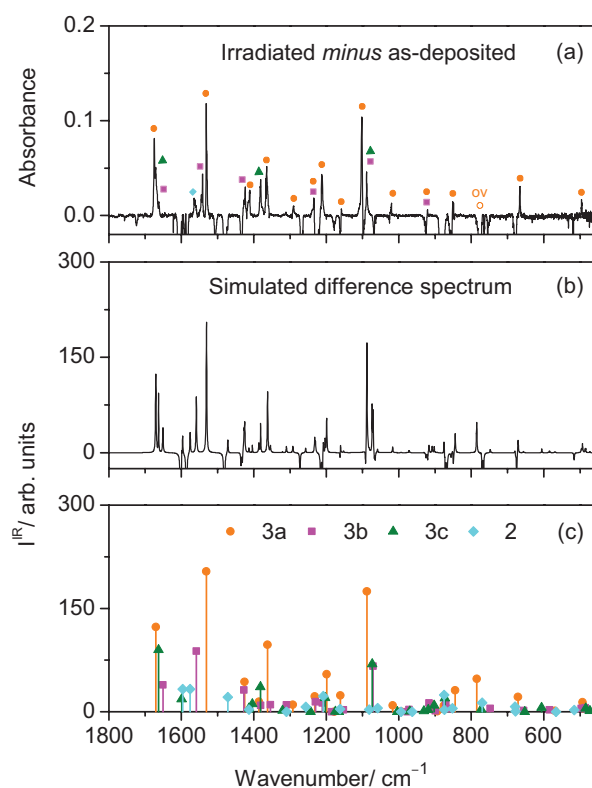
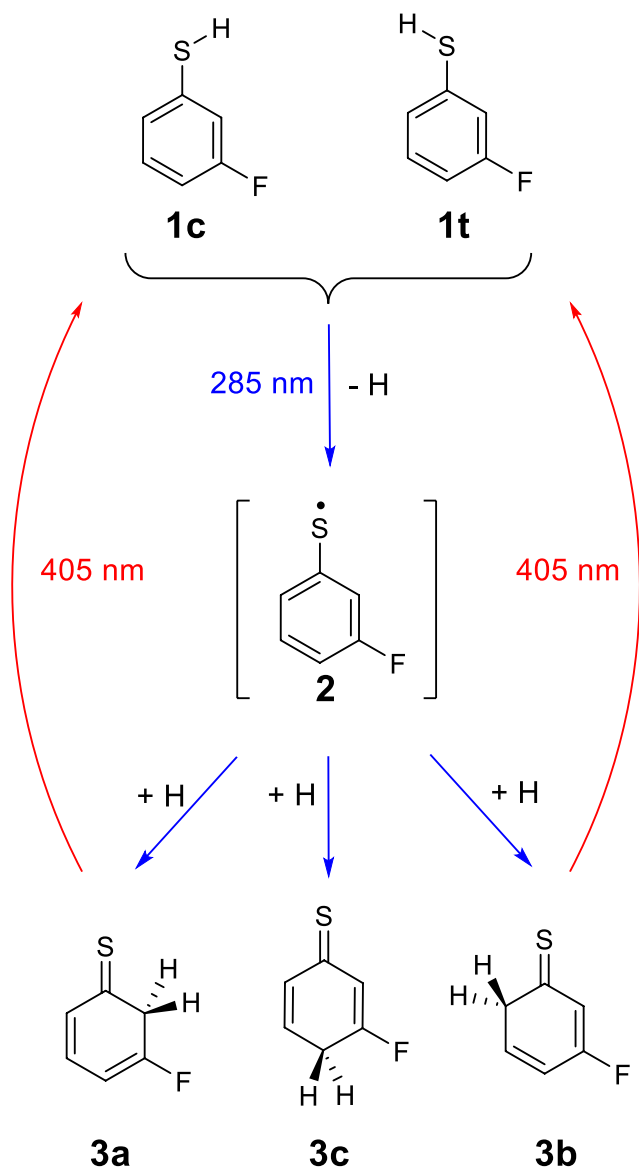


**FIGURE 2** | (a) IR difference spectrum (matrix irradiated for 2 min. at  $\lambda = 285$  nm *minus* as-deposited N<sub>2</sub> matrix) (16 K) in the 1800–450 cm<sup>-1</sup> region (the negative bands due to the reactant were truncated); (b) B3LYP/6–311++G(2d,2p) Simulated difference IR spectrum obtained by subtracting the theoretical spectrum of **1** from the combined spectra of photoproducts **3a**, **3b**, **3c**, and **2**. The spectrum simulation was performed as described in Section 2.2, with the wavenumbers scaled by 0.980 and intensities of **3a:3b:3c:2** scaled by 1:0.35:0.35:0.35, respectively, to achieve a better fit with the experimental data; (c) Vibrational data computed for the photoproducts (both wavenumbers and intensities were scaled). The medium intensity absorption predicted for **3a** at 785.1 cm<sup>-1</sup> (see Table 3) is not experimentally observed in the experimental spectrum because it is overlapped (ov) with bands of the reactant.

difference spectra shown in Figure 2b and the individual spectra shown in Figure 2c, have been scaled with intensity factors of 1.0, 0.35, 0.35, and 0.35, respectively (see caption of Figure 2 for details). Furthermore, selected regions of the experimental and theoretical spectra have been provided in Figure S3 to enhance the clarity of the identification of the different photoproducts.

The spectral comparison provides clear evidence that most of the emerging bands match those predicted for thione **3a**. In particular, the strongest new bands observed at 1675, 1531, and 1102 cm<sup>-1</sup> in the experimental difference spectrum are well reproduced by the most intense absorptions predicted for **3a** at 1670.5, 1530.7, and 1088.0 cm<sup>-1</sup> (*A*<sub>th</sub>  $\geq 97$  km mol<sup>-1</sup>), respectively, as detailed in Table S4. The good agreement between the experimental and theoretical spectra clearly confirms that thione **3a** is the dominant photoproduct formed during the UV irradiations at  $\lambda = 285$  nm.

Since the majority of the emerging IR bands are attributed to thione **3a**, confirming the presence of the other two thione isomers,



**SCHEME 1** | Photoinduced transformations observed for mFTP **1** isolated in a low-temperature  $N_2$  matrix.

**3b** and **3c**, presents a more significant challenge. For **3b**, four strong absorptions are predicted at 1651.0, 1558.8, 1427.2, and 1071.0  $\text{cm}^{-1}$  ( $A^{\text{th}} \geq 90 \text{ km mol}^{-1}$ , see Table S4). The first and third are predicted near spectral regions where **3a** also absorbs, complicating a definitive assignment to **3b**. However, the other two absorptions reproduce very well the new bands appearing at 1542 and 1089  $\text{cm}^{-1}$ , where **3a** shows no absorption, confirming that **3b** is also photogenerated. As for thione **3c**, its strongest calculated features are located at 1662.9, 1381.5, and 1073.5  $\text{cm}^{-1}$  ( $A^{\text{th}} \geq 100 \text{ km mol}^{-1}$ , Table S5). The first and last ones overlap with those assigned to thiones **3a** and **3b**, making differentiation more difficult. Nevertheless, the predicted feature at 1381.5  $\text{cm}^{-1}$  closely matches the medium-intensity band observed at 1382  $\text{cm}^{-1}$  where **3a** and **3b** absorb weakly, suggesting that **3c** may also be present, though its identification is less conclusive than that of **3a** and **3b**.

In addition, a weak band observed at 1565  $\text{cm}^{-1}$  cannot be accounted for by any of the three thione isomers. This band

is tentatively attributed to the strongest predicted absorption for the *meta*-fluorophenylthiyl radical **2** at 1575.8  $\text{cm}^{-1}$  ( $A^{\text{th}} = 94 \text{ km mol}^{-1}$ , see Table S5), which acts as an intermediate in the thiol-to-thione tautomerization process. There are additional four strong bands predicted for this species at 1596.4, 1471.9, 1208.4, and 874.9  $\text{cm}^{-1}$  ( $A^{\text{th}} \geq 65 \text{ km mol}^{-1}$ , see Table S5). However, all these bands overlap with those of the reactant, which limits the ability to definitively confirm the presence of the radical. Given that only a single band can be attributed to this species, its existence in the irradiated matrix remains uncertain and should be interpreted with caution.

Overall, the simulated IR difference spectrum, generated by subtracting the theoretical spectrum of mFTP **1** from the combined spectra of photoproducts **3a**, **3b**, **3c**, and **2**, provides an excellent fit with the experimental data. In Table 3 are listed the bands that emerged during the UV irradiations and their corresponding assignments to the photoproducts.

It is worth noting that, in the UV-induced photochemistry of thiophenol in an Ar matrix at  $\lambda = 290\text{--}287 \text{ nm}$ , in addition to the formation of thiones, the generation of thioketenes was also observed, resulting from the cleavage of the C–C bond at the  $\alpha$ -position relative to the C=S group in the *ortho*-thione [11]. This secondary reaction was spectroscopically identified by the appearance of a well-defined band at  $\sim 1740 \text{ cm}^{-1}$ , attributed to the antisymmetric stretching vibration of the C=C=S group. However, in the current study, no such new band was detected in the proximity of this spectral position during the irradiation of matrix-isolated **1** (see Figure 2), suggesting that this secondary process does not occur for **1** under the experimental conditions employed. The absence of bands in this region (see Figure 2) also rules out the formation of a five-membered ring thioketene as previously observed in the UV-induced photochemistry of 2-chlorothiophenol in a Ne matrix, where the antisymmetric C=C=S stretching vibration for this species was identified at 1759  $\text{cm}^{-1}$  [18], which is close to the position of the same band observed for this species isolated in an Ar matrix (1750  $\text{cm}^{-1}$ ) [64].

Following the irradiations at  $\lambda = 285 \text{ nm}$ , which led to the consumption of **1** and the formation of **3a**, **3b** and possibly **3c**, the  $N_2$  matrix was subjected to a series of additional irradiations at longer wavelengths. The objective was to selectively induce photoreactions in the thione isomers without affecting **1**. These irradiations were carried out in the  $\lambda = 425\text{--}390 \text{ nm}$  range, where thiones are expected to absorb, while **1** remains unaffected, as indicated by the TD-DFT simulated absorption spectra of all species provided in Figure S4. Among the thiones, only **3a** and **3b** are expected to photoreact within this wavelength range due to their strong predicted absorption near 400 nm. In contrast, **3c** is anticipated to absorb at shorter wavelengths, based on its simulated TD-DFT spectrum and the photochemical behavior of the analogous unsubstituted dione, which was found to photoreact at  $\lambda \leq 332 \text{ nm}$  [11], rendering **3c** unreactive under the current irradiation conditions. The only observed phototransformation induced by these irradiations was the partial reconversion of thiones **3a** and **3b** back to **1**, as indicated by the spectral changes shown in Figure 3, demonstrating that the thiol  $\leftrightarrow$  thione tautomerization process is reversible under these conditions (Scheme 1). This behavior is consistent with the

**TABLE 3** | Experimental and computed infrared absorptions of the photoproducts generated by irradiation at  $\lambda = 285$  nm of mFTP **1** isolated in an  $N_2$  matrix at 16 K.

Experimental ( $N_2$ , 16 K) <sup>a</sup>		Calculated <sup>b</sup>		Sym.	Approximate description <sup>c</sup>
$\tilde{\nu}$	Int.	$\tilde{\nu}^b$	$A^{th}$		
<b>5-fluorocyclohexa-2,4-diene-1-thione (3a)</b>					
1675/1671/1662	s	1670.5	123.2	A'	$\nu_{CC}$
1531	s	1530.7	203.8	A'	$\nu_{CC}$
1424/1412	m	1425.2	43.4	A'	$\delta_{CH}$
1365	m	1362.1	97.2	A'	$\omega_{CH_2}$ ; $\delta_{CH}$ ; $\nu_{CC}$
1291	w	1292.4	10.4	A'	$\omega_{CH_2}$ ; $\delta_{CH}$
1234	w	1232.1	22.1	A'	$\nu_{CC}$ ; $\delta_{CH}$
1213	m	1199.2	54.4	A'	$\nu_{CF} + \nu_{CS}$
1159	w	1161.0	23.4	A'	$\nu_{CC}$ ; $\delta_{CH}$
1102	s	1088.0	147.7	A'	$\nu_{CF} - \nu_{CS}$
1021	w	1017.0	9.2	A'	$\nu_{CC}$ ; $\delta_R$ ; $\delta_{CH}$
921	w	907.9	10.4	A'	$\delta_R$
851	w	844.4	31.0	A'	$\nu_{CC}$ ; $\nu_{CF}$
n.o.	—	785.1	47.6	A''	$\gamma_{CH}$
666	w	671.0	21.7	A'	$\delta_R$ ; $\nu_{CC}$ ; $\nu_{CS}$
496	w	493.3	13.9	A'	$\delta_R$
<b>3-fluorocyclohexa-2,4-diene-1-thione (3b)</b>					
1675/1671/1662	s	1651.0	111.3	A'	$\nu_{CC}$
1542	m	1558.8	251.8	A'	$\nu_{CC}$
1424/1412	m	1427.2	90.1	A'	$\delta_{CH}$ ; $\nu_{CC}$
1089	m	1071.0	189.1	A'	$\nu_{CF} - \nu_{CS}$
921	w	916.9	36.3	A'	$\nu_{CC}$ ; $\nu_{CS}$
<b>3-fluorocyclohexa-2,5-diene-1-thione (3c)</b>					
1675/1671/1662	s	1662.9	256.5	A'	$\nu_{CC}$
1382	m	1381.5	103.1	A'	$\omega_{CH_2}$ ; $\nu_{CC}$ ; $\delta_{CH}$
1089	m	1073.5	198.1	A'	$\nu_{CF} - \nu_{CS}$

Abbreviations: n.o. = not observed due to overlap with bands of the reactant. The experimental intensities (Int.) are expressed qualitatively: m = medium; s = strong; w = weak.

<sup>a</sup>Experimental data corresponds to the positions of the emerging bands ( $cm^{-1}$ ). For the split bands, the bolded band component is tentatively assigned to the corresponding thione.

<sup>b</sup>Calculated harmonic wavenumbers were multiplied by 0.980.

<sup>c</sup> $\nu$ , stretching;  $\delta$ , in-plane bending;  $\gamma$ , out-of-plane bending;  $\omega$ , wagging. Signs “+” and “-” designate combination of vibrations occurring in the same phase and in the opposite phase, respectively.

photoreversibility observed in thiophenol [11] and analogous compounds [22, 24].

### 3.3 | Vertical Excitations and Excited State Properties of mFTP

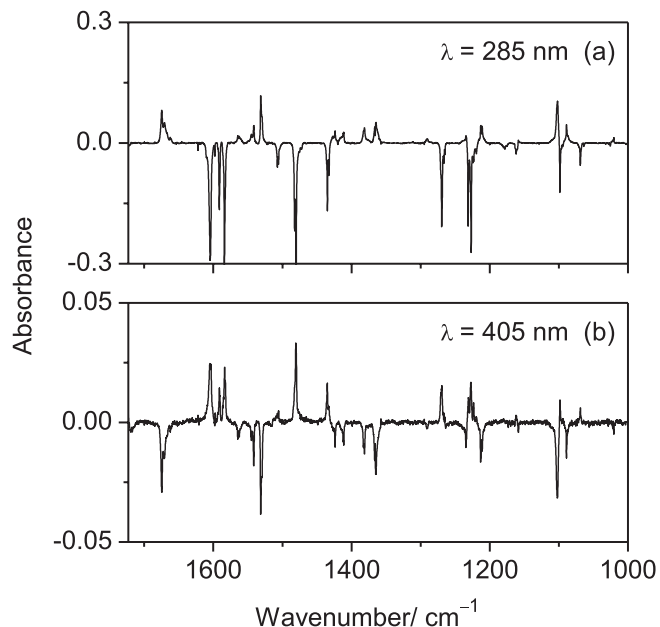
The computed vertical excitation energies, oscillator strengths, and main configuration weights for the three lowest singlet excited states ( $S_1$ ,  $S_2$ , and  $S_3$ ) of **1c** are presented in Table 4. This

table offers a direct comparison of the results obtained from CASPT2 with those derived from CASSCF, MR-CIS, and various TD-DFT methods, providing insights into the performance of each computational method in describing the excited-state properties of **1c**.

According to the calculations, the first excited state ( $S_1$ ) has  $A'$  symmetry and is at approximately 4.58 eV (at the CASPT2 level), in good agreement with the previously reported CASPT2/aug(S)-AVTZ value of 4.39 eV [8]. This calculated energy is also



close to the energy used in the experimental photoexcitation of the matrix-isolated compound (4.35 eV, see Section 3.2). Such agreement supports the quality of the computational approach



**FIGURE 3** | Spectral indication of the reversibility of the thiol ↔ thione phototautomerization. (a) Fragment of the difference obtained by subtracting the spectrum of the freshly deposited N<sub>2</sub> matrix from that recorded after irradiation at λ = 285 nm. (b) Fragment of the difference obtained by subtracting the spectrum recorded after irradiation at λ = 285 nm from the spectrum recorded after subsequent irradiation at λ = 405 nm.

in capturing the energetic properties relevant to the experimentally observed photochemistry. This state corresponds to a predominantly  $\pi\pi^*$  excitation, mixed with  $n_\pi\pi^*$ , as indicated by the configuration weights. The second state ( $S_2$ ) has A'' symmetry and is mainly described as a  $n_\pi\sigma^*$  state (see Table S7). The orbital involved in the electronic transition of  $S_2$  state is  $6a''$  (see Table S7), which can be characterized as a mixture of the  $n$  orbital of S and the  $\pi$  orbital of the ring. Despite the  $n_\pi\sigma^*$  description for  $S_2$ , it is important to point out that the former orbital is not a pure  $n$  orbital. This notation can also be found in Reference [16]. The CASPT2 vertical excitation energy of  $S_2$  is computed at ~5.28 eV, in agreement with the previously reported CASPT2/aug(S)-AVTZ value (4.99 eV) [8]. The third state ( $S_3$ ), assigned at ~5.29 eV and having A' symmetry, is mainly characterized by a  $n_\pi\pi^*$  excitation (see Table 4).

A comparison of the excitation energies obtained at the CASSCF, MR-CIS, and CASPT2 multireference/multiconfigurational levels shows a good overall agreement between the three methods. Considering that CASPT2 has shown a more trustworthy result concerning the analysis of the excited state properties, the discussion below concerning the accuracy of the other methods will be based on a direct comparison to it.

For  $S_1$ , the vertical excitation energies calculated at the CASSCF and MR-CIS levels are only slightly higher than those obtained at the CASPT2 level, with deviations of 0.27 and 0.25 eV, respectively, giving a mean deviation of about 6%. The difference between CASSCF and MR-CIS for this state is very small, only 0.02 eV. For  $S_2$ , the CASPT2 result is 0.4 and 0.18 eV lower than the CASSCF and MR-CIS values, respectively. MR-CIS and CASPT2 are in excellent agreement (mean deviation of

**TABLE 4** | Vertical excitation energies, oscillator strengths and main configuration weights for each state computed at CASSCF, MR-CIS, and CASPT2 levels with the aug-cc-pVDZ basis for **1c**.

States	Weights <sup>a</sup>	$\Delta E$	$f^b$	Weights <sup>a</sup>	$\Delta E$	$f^b$
	CASPT2			TD- $\tau$ -HCTHhyb		
$S_0$ (A')	0.96gs	—	—	0.86gs	—	—
$S_1$ (A')	0.61( $\pi_3\pi_1^*$ )	4.58	0.028	0.57( $\pi_3\pi_1^*$ ) + 0.33( $n_\pi\pi_2^*$ )	4.70	0.032
$S_2$ (A'')	0.76( $n_\pi\sigma_1^*$ )	5.28	0.019	0.69( $n_\pi\sigma_1^*$ )	4.94	0.001
$S_3$ (A')	0.78( $n_\pi\pi_1^*$ )	5.29	0.197	0.55( $n_\pi\pi_1^*$ )	5.18	0.193
	CASSCF(12,11)			TD- $\omega$ B97XD		
$S_0$ (A')	0.87gs	—	—	0.83gs	—	—
$S_1$ (A')	0.36( $\pi_3\pi_1^*$ ) + 0.31( $n_\pi\pi_2^*$ )	4.85	0.034	0.51( $\pi_3\pi_1^*$ ) + 0.34( $n_\pi\pi_2^*$ )	5.04	0.034
$S_2$ (A'')	0.77( $n_\pi\sigma_1^*$ )	5.68	0.014	0.43( $n_\pi\sigma_1^*$ )	5.26	0.001
$S_3$ (A')	0.77( $n_\pi\pi_1^*$ )	5.92	0.185	0.49( $n_\pi\pi_1^*$ )	5.52	0.186
	MR-CIS			TD-M062X		
$S_0$ (A')	0.89gs	—	—	0.85gs	—	—
$S_1$ (A')	0.48( $\pi_3\pi_1^*$ ) + 0.39( $n_\pi\pi_2^*$ )	4.83	0.035	0.44( $\pi_3\pi_1^*$ ) + 0.33( $n_\pi\pi_2^*$ )	5.02	0.002
$S_2$ (A'')	0.81( $n_\pi\sigma_1^*$ )	5.46	0.012	0.54( $n_\pi\sigma_1^*$ )	5.04	0.041
$S_3$ (A')	0.81( $n_\pi\pi_1^*$ )	5.42	0.191	0.43( $n_\pi\pi_1^*$ )	5.68	0.017

<sup>a</sup>Only weights of the CSFs which are larger than 0.1 are shown.

<sup>b</sup>Oscillator strength.

3.4%), whereas CASSCF deviates more significantly (7.8%). Regarding  $S_3$ , the MR-CIS result is only 0.13 eV higher than that of CASPT2, corresponding to a deviation of 2.5%. Although the nature of  $S_3$  is correctly described at the CASSCF level, it shows a larger discrepancy compared to CASPT2, differing by 0.63 eV, corresponding to a deviation of 11.9%. Overall, all multireference/multiconfigurational methods show a good performance for all three excited singlet states of mFTP, with  $S_3$  being the state for which the computed oscillator strength is the largest at all computational levels. MR-CIS showed very good agreement with CASPT2 for all excited-state properties of the studied system, reflecting the importance of dynamic electron correlation. CASSCF performed slightly worse in terms of excitation energy values, although it provided a reliable characterization of the states' nature.

The excitation energies computed at the TD-DFT level are in good agreement with those obtained from CASPT2, as shown in Table 4. The nature of the excited states is correctly described, and the weights of the main configurations agree among all three functionals. Concerning the oscillator strength values, only TD-M062X deviated significantly, predicting  $S_2$  as the most intense state rather than  $S_3$ . Both TD- $\omega$ B97XD and TD- $\tau$ -HCTHhyb functionals showed reasonable agreement with the  $f$  values computed at the CASPT2 level, although they slightly overestimated these values for  $S_1$ . Concerning  $S_2$  oscillator strength values, TD- $\omega$ B97XD and TD- $\tau$ -HCTHhyb results are in agreement with CASPT2 predictions, however they were numerically smaller. TD-M062X predicts a higher intensity, been not able to correctly assign the  $f$  values for  $S_2$ . Consistently,  $S_3$  displayed the highest oscillator strength for both CASPT2 and TD-DFT methods, matching predictions from previous multireference results [16]. Regarding excitation energies, the TD- $\tau$ -HCTHhyb functional performed very well for all three states, with energy deviations of 0.12, 0.38, and 0.11 eV from CASPT2 values, corresponding to errors of 2.6%, 7.2%, and 2.1%, respectively. This result was already expected as a previous benchmark study of TD-DFT functionals for the thiophenol molecule had indicated a promising performance for the TD- $\tau$ -HCTHhyb functional [28]. The TD- $\omega$ B97XD functional performed slightly worse than TD- $\tau$ -HCTHhyb with larger errors for the energies (differences of 0.46, 0.02, and 0.23 eV), showing better results only for  $S_2$ . Lastly, the TD-M062X functional showed the worse result in comparison with the other functionals applied in the study (0.44, 0.28, 0.39 eV) and, as discussed before, it was not able to correctly assign the relative intensity of the  $S_3$  state. These results support the reliability of the TD- $\tau$ -HCTHhyb functional for the absorption spectrum simulation based on dynamic calculations.

Based on the deviations from CASPT2 excitation energy values, as well as on the ability of the methods to predict the correct nature of the states, they can be ranked in descending order as follows: MR-CIS>TD- $\tau$ -HCTHhyb>CASSCF>TD- $\omega$ B97XD>TD-M062X.

### 3.4 | Photoabsorption Spectra

The UV-photoabsorption spectrum simulated for **1c** is shown in Figure 4. The TD- $\tau$ -HCTHhyb method was selected for

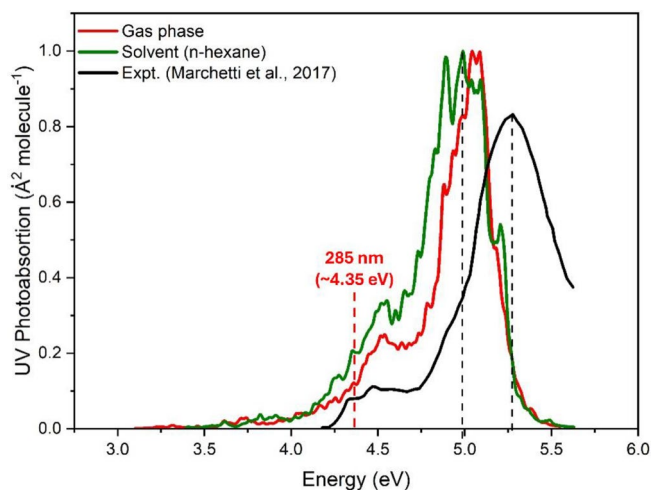


**FIGURE 4** | Absorption cross sections of **1c** calculated at the TD- $\tau$ -HCTHhyb/aug-cc-pVDZ level in gas phase and solvent in comparison to available experimental data [8]. The dotted vertical black lines indicate the estimated maximum of the highest energy band. The dotted vertical red line indicates the irradiation energy used in this work.

spectrum simulations due to its good agreement with the CASPT2 results for vertical excitation energies. Marchetti et al. have obtained the UV photoabsorption spectrum in *n*-hexane solution, at room temperature, in the range 4.13–5.64 eV (220 to 300 nm). As can be seen from Figure 4 the experimental spectrum exhibits two bands in this region, one broader and more intense, with the maximum around 5.25 eV and the other with the maximum around 4.50 eV. The photoabsorption spectrum of the *ortho*-fluorothiophenol in *n*-hexane solution has also been reported [10]. As a further test for the methodology used to simulate the absorption spectrum, based on the nuclear ensemble approach explained before, it has also been applied to simulate the photoabsorption spectrum of the *ortho*-fluorothiophenol in *n*-hexane, also yielding good results.

In the region up to 5.5 eV, the simulated gas phase spectrum of **1c** is composed of two bands, a small intensity one with maximum around 4.5 eV and another (more intense) band with maximum around 5.2 eV, thus exhibiting a similar pattern to that observed experimentally in *n*-hexane. The comparison of these spectral features with the vertical transitions allows their straightforward assignment, that is, the electronic transition  $\pi\pi^*$  ( $S_1$  state) corresponds to the lower energy band while  $n_\pi\sigma^*$  and  $n_\pi\pi^*$  ( $S_2$  and  $S_3$  states, respectively) are assigned to the second band.

As expected, due to the low polarity of the solvent, a small solvent effect has been predicted in the case of the simulated spectrum in *n*-hexane. The main differences compared to the data obtained for the gas phase are: (i) a small redshift of  $\sim$ 0.2 eV for the higher energy band; (ii) a small intensity gain for the lower energy band (see Figure 4). The spectrum simulated with the TD- $\tau$ -HCTHhyb functional (in *n*-hexane) shows good agreement with experimental data [8], though the higher energy band shows a small red-shift of  $\sim$ 0.25 eV compared to experiment, as it can be seen from the vertical dotted lines in Figure 4. Nevertheless, this difference can be considered very good given the accuracy of the TD-DFT methodology.

## 4 | Concluding Remarks

In this study, the IR spectrum of mFTP isolated in a low-temperature N<sub>2</sub> matrix was recorded and assigned for the first time, with support from B3LYP vibrational frequency calculations for the *cis* and *trans* conformers. Upon UV irradiation at 285 nm, the matrix-isolated compound showed significant photoreactivity, with approximately 60% of the compound converting into photoproducts, specifically thione isomers **3a**, **3b**, and **3c**, within just 2 min of irradiation. Spectroscopic analysis, supported by theoretical calculations, confirmed the formation of these isomers, with thione **3a** being the dominant product. The phototransformation was shown to correspond to thiol-to-thione tautomerizations, involving the hydrogen atom transfer from the SH group to the aromatic ring through a  $\pi\sigma^*$  mediated mechanism similar to that reported for phenols and other aromatic compounds [13]. Interestingly, no evidence of thioketene formation was observed under the given experimental conditions, distinguishing this reaction from similar photochemical processes in other thiophenol derivatives. Furthermore, additional irradiations at longer wavelengths (425–390 nm) demonstrated the reversibility of the tautomerization process, as the thione isomers (namely **3a** and **3b**) were found to convert back to the original thiol form. This reversible photochemistry highlights the dynamic nature of mFTP under UV light.

The vertical excitations and excited state properties of mFTP **1** were well-characterized across various computational levels, with MR-CIS and CASPT2 showing strong agreement and proving to be the most reliable methods for describing the excited states. The TD-DFT method, specifically the TD- $\tau$ -HCTHhyb functional, also performed well, with minimal deviations in excitation energies. Moreover, the simulated UV-photoabsorption spectrum displayed consistency with experimental data, particularly regarding solvent effects.

Overall, this combined experimental and theoretical study has expanded the understanding of the spectroscopic and photochemical properties of *meta*-fluorinated thiophenol, providing insights that can serve as a basis for investigating other substituted thiophenols.

### Acknowledgments

This work was supported by Project PTDC/QUI-QFI/1880/2020, funded by National Funds via the Portuguese Foundation for Science and Technology (FCT), and by the European research Agency via the European Research Agency ERA-Chair 1011848998 Spectroscopy@IKU “Manipulating and Characterizing Molecular Architectures: From Isolated Molecules to Molecular Crystals.” The Coimbra Chemistry Centre—Institute of Molecular Sciences (CQC-IMS) is supported by FCT through projects UIDB/00313/2020 and UIDP/00313/2020, co-funded by COMPETE and the IMS special complementary funds provided by FCT. The authors also acknowledge the Laboratory for Advanced Computing at University of Coimbra (<https://www.uc.pt/lca>) for providing computing resources and LaserLab Coimbra for experimental facilities. A. J. Lopes Jesus and J. R. Lucena Jr. would like to thank Igor Reva for his invaluable help with the matrix-isolation experiments and for insightful discussions in the early stages of this work. E. Ventura and S. A. do Monte. thank the Brazilian agency CNPq (Grant Numbers 308371/2021-6, and 313398/2023-2) for support. E. Ventura, S. A. do Monte, J. R. Lucena Jr. and G. P. Rodrigues thank funding

from the National Institute of Science and Technology on Molecular Sciences (INCT-CiMol) (Grant CNPq 406804/2022-2 and fellowships 153685/2024-7), CAPES, the Laboratório Nacional de Computação Científica—LNCC for the computational facilities of the Santos Dumont (SDumont) supercomputer cluster and the Brazilian agency FINEP for financial support. The authors celebrate Hans Lischka's 80th birthday and thank him for his valuable contributions to theoretical and computational quantum chemistry, which has allowed the expansion of collaborations between theoretical and experimental chemistry to solve complex problems.

### Data Availability Statement

The data that supports the findings of this study are available in the [Supporting Information](#) of this article.

### References

- I. S. Lim, J. S. Lim, Y. S. Lee, and S. K. Kim, “Experimental and Theoretical Study of the Photodissociation Reaction of Thiophenol at 243 nm: Intramolecular Orbital Alignment of the Phenylthiyl Radical,” *Journal of Chemical Physics* 126 (2007): 034306.
- A. L. Devine, M. G. Nix, R. N. Dixon, and M. N. Ashfold, “Near-Ultraviolet Photodissociation of Thiophenol,” *Journal of Physical Chemistry. A* 112 (2008): 9563–9574.
- J. S. Lim, Y. S. Lee, and S. K. Kim, “Control of Intramolecular Orbital Alignment in the Photodissociation of Thiophenol: Conformational Manipulation by Chemical Substitution,” *Angewandte Chemie, International Edition* 47 (2008): 1853–1856.
- J. S. Lim, I. S. Lim, K.-S. Lee, D.-S. Ahn, Y. S. Lee, and S. K. Kim, “Intramolecular Orbital Alignment Observed in the Photodissociation of [D<sub>1</sub>] Thiophenol,” *Angewandte Chemie, International Edition* 45 (2006): 6290–6293.
- J. S. Lim, H. Choi, I. S. Lim, S. B. Park, Y. S. Lee, and S. K. Kim, “Photodissociation Dynamics of Thiophenol-d1: The Nature of Excited Electronic States Along the S-D Bond Dissociation Coordinate,” *Journal of Physical Chemistry. A* 113 (2009): 10410–10416.
- H. An, H. Choi, Y. S. Lee, and K. K. Baek, “Factors Affecting the Branching Ratio of Photodissociation: Thiophenol Studied through Quantum Wavepacket Dynamics,” *ChemPhysChem* 16 (2015): 1529–1534.
- M. N. Ashfold, G. A. King, D. Murdock, M. G. Nix, T. A. Oliver, and A. G. Sage, “ $\pi\sigma^*$  Excited States in Molecular Photochemistry,” *Physical Chemistry Chemical Physics* 12 (2010): 1218–1238.
- B. Marchetti, T. N. V. Karsili, M. Cipriani, C. S. Hansen, and M. N. R. Ashfold, “The Near Ultraviolet Photodissociation Dynamics of 2- and 3-Substituted Thiophenols: Geometric vs. Electronic Structure Effects,” *Journal of Chemical Physics* 147 (2017): 013923.
- G.-S.-M. Lin, C. Xie, and D. Xie, “Nonadiabatic Effect in Photodissociation Dynamics of Thiophenol via the  $^1\pi\pi^*$  State,” *Journal of Physical Chemistry. A* 122 (2018): 5375–5382.
- J. S. Lim, H. S. You, S. Han, and S. K. Kim, “Photodissociation Dynamics of Ortho-Substituted Thiophenols at 243 nm,” *Journal of Physical Chemistry. A* 123 (2019): 2634–2639.
- I. Reva, M. J. Nowak, L. Lapinski, and R. Fausto, “Hydrogen Atom Transfer Reactions in Thiophenol: Photogeneration of Two New Thione Isomers,” *Physical Chemistry Chemical Physics* 17 (2015): 4888–4898.
- H. S. You, S. Han, J.-H. Yoon, et al., “Structure and Dynamic Role of Conical Intersections in the  $\pi\sigma^*$ -Mediated Photodissociation Reactions,” *International Reviews in Physical Chemistry* 34 (2015): 429–459.
- A. L. Sobolewski, W. Domcke, C. Dedonder-Lardeux, and C. Jouvet, “Excited-State Hydrogen Detachment and Hydrogen Transfer Driven by Repulsive  $^1\pi\sigma^*$  States: A New Paradigm for Nonradiative Decay in

- Aromatic Biomolecules,” *Physical Chemistry Chemical Physics* 4 (2002): 1093–1100.
14. S. Yamazaki, W. Domcke, and A. L. Sobolewski, “Nonradiative Decay Mechanisms of the Biologically Relevant Tautomer of Guanine,” *Journal of Physical Chemistry. A* 112 (2008): 11965–11968.
15. T. S. Venkatesan, S. G. Ramesh, Z. Lan, and W. Domcke, “Theoretical Analysis of Photoinduced H-Atom Elimination in Thiophenol,” *Journal of Chemical Physics* 136 (2012): 174312.
16. F. B. D. Lima, G. Pereira Rodrigues, J. R. de Lucena Júnior, et al., “A Comparative Multi-Reference Configuration Interaction Study of the Low-Lying States of Two Thione Isomers of Thiophenol,” *International Journal of Quantum Chemistry* 120 (2020): e26263.
17. V. Ovejas, M. Fernández-Fernández, R. Montero, and A. Longarte, “On the Ultrashort Lifetime of Electronically Excited Thiophenol,” *Chemical Physics Letters* 661 (2016): 206–209.
18. M. Hayashi, R. Ichihara, N. Akai, and M. Nakata, “Photoreaction of 2-Chlorothiophenol Studied by Low-Temperature Matrix-Isolation IR Spectroscopy with DFT Calculation,” *Journal of Molecular Structure* 1244 (2021): 130909.
19. B. M. Giuliano, I. Reva, L. Lapinski, and R. Fausto, “Infrared Spectra and Ultraviolet-Tunable Laser Induced Photochemistry of Matrix-Isolated Phenol and Phenol-d5,” *Journal of Chemical Physics* 136 (2012): 024505.
20. I. Reva, L. Lapinski, A. J. Lopes Jesus, and M. J. Nowak, “Photoinduced Transformations of Indole and 3-Formylindole Monomers Isolated in Low-Temperature Matrices,” *Journal of Chemical Physics* 147 (2017): 194304.
21. I. Reva, A. J. L. Jesus, C. M. Nunes, J. P. L. Roque, and R. Fausto, “UV-Induced Photochemistry of 1,3-Benzoxazole, 2-Isocyanophenol, and 2-Cyanophenol Isolated in Low-Temperature Ar Matrixes,” *Journal of Organic Chemistry* 86 (2021): 6126–6137.
22. H. Rostkowska, L. Lapinski, I. Reva, B. J. A. N. Almeida, M. J. Nowak, and R. Fausto, “UV-Induced Hydrogen-Atom Transfer in 3,6-Dithiopyridazine and in Model Compounds 2-Thiopyridine and 3-Thiopyridazine,” *Journal of Physical Chemistry. A* 115 (2011): 12142–12149.
23. A. J. Lopes Jesus, J. R. de Lucena Júnior, R. Fausto, and I. Reva, “Infrared Spectra and Phototransformations of *Meta*-Fluorophenol Isolated in Argon and Nitrogen Matrices,” *Molecules* 27 (2022): 8248.
24. A. Khvorostov, L. Lapinski, H. Rostkowska, and M. J. Nowak, “Unimolecular Photochemistry of 4-Thiouracils,” *Journal of Photochemistry and Photobiology. B* 81 (2005): 1205–1211.
25. C. M. Nunes, I. Reva, R. Fausto, D. Bégué, and C. Wentrup, “Bond-Shift Isomers: The Co-Existence of Allenic and Propargylic Phenylnitrite Imines,” *ChemComm* 51 (2015): 14712–14715.
26. C. M. Nunes, A. J. Lopes Jesus, M. T. S. Rosado, and R. Fausto, “On the Carbenic Nature of Nitrile Ylides: Experimental and Computational Characterization of Hydroxy and Amino Nitrile Ylides,” *European Journal of Organic Chemistry* 27 (2024): e202301103.
27. K. C. Woo and S. K. Kim, “Real-Time Tunneling Dynamics through Adiabatic Potential Energy Surfaces Shaped by a Conical Intersection,” *Journal of Physical Chemistry Letters* 11 (2020): 6730–6736.
28. F. B. d. Lima, “Theoretical Study of Photoinduced Hydrogen Transfer in Thiophenol and Some of Its Derivatives (2020). PhD thesis, Department of Chemistry; Federal University of Paraíba: João Pessoa-PB, Brazil, <https://repositorio.ufpb.br/jspui/handle/123456789/18447>.
29. S. Han, H. S. You, S. Y. Kim, and S. K. Kim, “Dynamic Role of the Intramolecular Hydrogen Bonding in Nonadiabatic Chemistry Revealed in the UV Photodissociation Reactions of 2-Fluorothiophenol and 2-Chlorothiophenol,” *Journal of Physical Chemistry. A* 118 (2014): 6940–6949.
30. J. Ning and D. G. Truhlar, “Electronic Excitation of ortho-Fluorothiophenol,” *Journal of Physical Chemistry. A* 127 (2023): 1469–1474.
31. T. Takakura, K. Fujioka, M. Okuyama, and H. Kamada, “Flash Photolysis of Aromatic Thiols in Aqueous Solution,” *Journal of Spectroscopic Society of Japan* 24 (1975): 287–290.
32. C. Lee, W. Yang, and R. G. Parr, “Development of the Colle-Salvetti Correlation-Energy Formula into a Functional of the Electron Density,” *Physical Review B* 37 (1988): 785–789.
33. S. H. Vosko, L. Wilk, and M. Nusair, “Accurate Spin-Dependent Electron Liquid Correlation Energies for Local Spin Density Calculations: A Critical Analysis,” *Canadian Journal of Physics* 58 (1980): 1200–1211.
34. A. D. Becke, “Density-functional exchange-energy approximation with correct asymptotic behavior,” *Physical Review A* 38 (1988): 3098–3100.
35. M. J. Frisch, J. A. Pople, and J. S. Binkley, “Self-Consistent Molecular Orbital Methods 25. Supplementary Functions for Gaussian Basis Sets,” *Journal of Chemical Physics* 80 (1984): 3265–3269.
36. G. A. C. Zhurko, “Chemcraft, Version 1.8,” accessed October, 2024, <http://www.chemcraftprog.com>.
37. C. Møller and M. S. Plesset, “Note on an Approximation Treatment for Many-Electron Systems,” *Physical Review A* 46 (1934): 618–622.
38. R. A. Kendall, T. H. Dunning, Jr., and R. J. Harrison, “Electron Affinities of the First-Row Atoms Revisited. Systematic Basis Sets and Wave Functions,” *Journal of Chemical Physics* 96 (1992): 6796–6806.
39. M. J. Frisch, G. W. Trucks, H. B. Schlegel, et al., “Molecular Modeling and Synthesis of Ethyl Benzyl Carbamates as Possible Ixodicide Activity,” *Computational Chemistry* 1, no. 7 (2016).
40. H. Lischka, R. Shepard, I. Shavitt, et al., “COLUMBUS, an Ab Initio Electronic Structure Program,” release 7.2. 2022.
41. H. Lischka, T. Müller, P. G. Szalay, I. Shavitt, R. M. Pitzer, and R. Shepard, “Columbus—a Program System for Advanced Multireference Theory Calculations,” *Wiley Interdisciplinary Reviews: Computational Molecular Science* 1 (2011): 191–199.
42. H. Lischka, R. Shepard, R. M. Pitzer, et al., “High-level multireference methods in the quantum-chemistry program system COLUMBUS: Analytic MR-CISD and MR-AQCC gradients and MR-AQCC-LRT for excited states, GUGA spin-orbit CI and parallel CI density,” *Physical Chemistry Chemical Physics* 3 (2001): 664–673.
43. “TURBOMOLE V7.4 2019, A Development of (University of Karlsruhe) and (Forschungszentrum Karlsruhe GmbH), 1989–2007. TURBOMOLE GmbH, Since 2007,” <http://www.turbomole.com>.
44. M. J. Frisch, G. W. Trucks, H. B. Schlegel, et al., “Redshift of Excitation Wavelength Caused by the Concentration of L-Tryptophan in Water: A Theoretical and Experimental Study,” *Open Journal of Physical Chemistry* 11, no. 2 (2021).
45. J.-D. Chai and M. Head-Gordon, “Long-range corrected hybrid density functionals with damped atom–atom dispersion corrections,” *Physical Chemistry Chemical Physics* 10 (2008): 6615–6620.
46. Y. Zhao and D. G. Truhlar, “The M06 Suite of Density Functionals for Main Group Thermochemistry, Thermochemical Kinetics, Noncovalent Interactions, Excited States, and Transition Elements: Two New Functionals and Systematic Testing of Four M06-Class Functionals and 12 Other Fun,” *Theoretical Chemistry Accounts* 120 (2008): 215–241.
47. A. D. Boese and N. C. Handy, “New Exchange-Correlation Density Functionals: The Role of the Kinetic-Energy Density,” *Journal of Chemical Physics* 116 (2002): 9559–9569.
48. T. H. Dunning, Jr., “Gaussian basis sets for use in correlated molecular calculations. I. The atoms boron through neon and hydrogen,” *Journal of Chemical Physics* 90 (1989): 1007–1023.
49. D. E. Woon, T. H. Dunning, and Jr., “Gaussian basis sets for use in correlated molecular calculations. IV. Calculation of static electrical response properties,” *Journal of Chemical Physics* 100 (1994): 2975–2988.

50. Y. Takano and K. N. Houk, "Benchmarking the Conductor-like Polarizable Continuum Model (CPCM) for Aqueous Solvation Free Energies of Neutral and Ionic Organic Molecules," *Journal of Chemical Theory and Computation* 1 (2005): 70–77.
51. M. Barbatti, M. Bondanza, R. Crespo-Otero, et al., "Newton-X Platform: New Software Developments for Surface Hopping and Nuclear Ensembles," *Journal of Chemical Theory and Computation* 18 (2022): 6851–6865.
52. M. E. Casida and M. Huix-Rotllant, "Progress in Time-Dependent Density-Functional Theory," *Annual Review of Physical Chemistry* 63 (2012): 287–323.
53. W. Sun and J. van Wijngaarden, "Structural Elucidation of 2-Fluorothiophenol from Fourier Transform Microwave Spectra and Ab Initio Calculations," *Journal of Molecular Structure* 1144 (2017): 496–501.
54. W. G. Barbosa, C. V. Santos-Jr, R. B. Andrade, J. R. Lucena, Jr., and R. T. Moura, Jr., "Bond Analysis in Meta- and Para-Substituted Thiophenols: Overlap Descriptors, Local Mode Analysis, and QTAIM," *Journal of Molecular Modeling* 30 (2024): 139.
55. A. J. Lopes Jesus, M. T. S. Rosado, I. Reva, R. Fausto, M. E. S. Eusébio, and J. S. Redinha, "Structure of Isolated 1,4-Butanediol: Combination of MP2 Calculations, NBO Analysis, and Matrix-Isolation Infrared Spectroscopy," *Journal of Physical Chemistry. A* 112 (2008): 4669–4678.
56. M. T. S. Rosado, A. J. Lopes Jesus, I. D. Reva, R. Fausto, and J. Redinha, "Conformational Cooling Dynamics in Matrix-Isolated 1,3-Butanediol," *Journal of Physical Chemistry A* 113 (2009): 7499–7507.
57. A. J. Lopes Jesus, M. T. S. Rosado, I. Reva, R. Fausto, M. E. Eusébio, and J. Redinha, "Conformational Study of Monomeric 2,3-Butanediols by Matrix-Isolation Infrared Spectroscopy and DFT Calculations," *Journal of Physical Chemistry A* 110 (2006): 4169–4179.
58. K. Grzechnik, K. Rutkowski, and Z. Mielke, "The S–H...N Versus O–H...N Hydrogen Bonding in the Ammonia Complexes with CH<sub>3</sub>OH and CH<sub>3</sub>SH," *Journal of Molecular Structure* 1009 (2012): 96–102.
59. S. Lopes, A. V. Domanskaya, R. Fausto, M. Räsänen, and L. Khrichtchev, "Formic and Acetic Acids in a Nitrogen Matrix: Enhanced Stability of the Higher-Energy Conformer," *Journal of Chemical Physics* 133 (2010): 144507.
60. A. J. Lopes Jesus, C. M. Nunes, and I. Reva, "Conformational Structure, Infrared Spectra and Light-Induced Transformations of Thymol Isolated in Noble Gas Cryomatrices," *Photochemistry* 2 (2022): 405–422.
61. A. J. Lopes Jesus, R. Fausto, and I. Reva, "Conformational Space, IR-Induced, and UV-Induced Chemistry of Carvacrol Isolated in a Low-Temperature Argon Matrix," *Journal of Physical Chemistry. A* 125 (2021): 8215–8229.
62. A. K. Chandra, P.-C. Nam, and M. T. Nguyen, "The S–H Bond Dissociation Enthalpies and Acidities of Para and Meta Substituted Thiophenols: A Quantum Chemical Study," *Journal of Physical Chemistry. A* 107 (2003): 9182–9188.
63. J. Rimarčík, V. Lukeš, E. Klein, and L. Rottmannová, "On the Enthalpies of Homolytic and Heterolytic S–H Bond Cleavage in Para and Meta Substituted Thiophenols," *Computational and Theoretical Chemistry* 967 (2011): 273–283.
64. T. Jørgensen, C. T. Pedersen, R. Flammang, and C. Wentrup, "Formation of Thioketenes by Thermal Fragmentation of 1, 2-Dithiol-3-Ones," *Journal of the Chemical Society, Perkin Transactions 2* (1997): 173–178.

### Supporting Information

Additional supporting information can be found online in the Supporting Information section.